J Mater Sci

Computation & theory

Structural, thermodynamic, electronic, and optical properties of β-BeO phase ZnO under negative pressure: a first-principles study

Muhammad Adnan Kamboh[1], Lei Hao[1], Muhammad Farhan[2], Yanan Su[1], Lirui Wang[1], Qili Chen[1], Hai Wang[1], Jiying Zhang[3,4], and Qingbo Wang[1,*]

[1] *School of Mathematics and Physics, China University of Geosciences (Wuhan), Lumo Road, Wuhan 430074, People's Republic of China*

[2] *Department of Mechanical Engineering, NED University of Engineering, Science and Technology, Karachi, Pakistan*

[3] *State Key Laboratory of Precision Blasting, Jianghan University, Wuhan 430056, People's Republic of China*

[4] *Key Laboratory of Optoelectronic Chemical Materials and Devices, School of Chemical and Environmental Engineering, Jianghan University, Ministry of Education, Wuhan 430056, People's Republic of China*

Received: 23 May 2022

Accepted: 1 October 2022

© The Author(s), under exclusive licence to Springer Science+Business Media, LLC, part of Springer Nature 2022

ABSTRACT

This study presents the structural, thermodynamic, electronic, and optical properties of the β-BeO phase of ZnO under negative pressure calculated via first-principles method. We analyzed the phase transition by the local density approximation, and we find that the structural phase transition from wurtzite B4 to metastable β-BeO phase occurred at -10.2 GPa. We used the Debye model to calculate the thermodynamic properties. The results show that the bulk modulus decreases with increasing temperature or decreasing pressure whereas the heat capacity and thermal expansion coefficient increase with increasing temperature or decreasing pressure. We employed the hybrid functional (Becke-Lee-Young-Parr exchange–correlation functional) method to predict the electronic and optical properties. The band structure calculations confirmed that the β-BeO phase possesses an indirect wider band gap than that of B4 phase. Redshift in band gap energy and optical properties are observed with decreasing pressure. The dielectric function $\varepsilon_1(\omega)$ calculations validate that the β-BeO phase exhibits metallic behaviour at around 16.3 eV, whereas optical constants exploration has confirmed its transparent nature. The present study proves that the β-BeO phase ZnO may be potentially applicable in next-generation electronics. Additionally, it is helpful in material sciences to understand and examine the surrounding pressure during a variety of mineral formation processes.

Handling Editor: Yaroslava Yingling.

Address correspondence to E-mail: qingbowang@cug.edu.cn

https://doi.org/10.1007/s10853-022-07816-2

Published online: 14 October 2022

Introduction

Energy conversion and storage materials have specific requirements on material band gaps, for example, thermoelectric materials generally demand the band gaps are smaller than 1 eV [1–3]. Recently, ZnO has been extensively studied under pressure due to its wide band gap and outstanding optical properties [4–8]. It has emerged as a prominent semiconductor with various technological applications, including piezoelectric devices [9], optoelectronic devices [10, 11], solar cells [12], photodetectors [13], photocatalyst [14], energy generation devices [15], energy storage devices [16] and thermoelectric devices [17]. ZnO is found as a rare mineral zincite that exhibits a hexagonal structure [18, 19]. At ambient conditions, its wurtzite (B4) type structure is found to be potentially stable. It is known that the application of external pressure induces a substantial change in the crystal structure as well as the thermodynamic, electronic, and optical properties of materials [20]. Hence, lots of works studied on the phase transitions and the properties of ZnO have been carried out [21–27] by using experimental techniques, computational methods [28, 29], and pressure equipment [30].

Experimental investigations using x-ray diffraction and Mössbauer spectroscopy techniques revealed that the wurtzite (B4) phase ZnO can transform into the rock salt (B1) phase ZnO by applying high pressure [31–33]. Meanwhile, several theoretical studies have also found the pressure-induced direct transition of the B4 phase to the B1 (wurtzite), B2 (CsCl), B3 (zinc blende), and B10 (PbO) phase ZnO [34–38]. The search for new possible transition routes of the wurtzite (B4) ZnO and its intermediary phases are a focused area in the material sciences. Molepo et al. predicted potential BN (B_k) and NiAs ($B8_1$) type modifications in ZnO structure at high pressure [39]. Zhenwei Li et al. using ab-initio calculations proposed PbO (B10) type intermediary structure in the transition route from the B1 to B2 phase [40]. Until now, studies have focused mostly on characterizing the phase transitions in ZnO and their accompanied properties under high pressure. Recently Zagorac et al. proposed a new intermediate β-beryllium oxide (β-BeO) type structure in the transition route from B4 to B2 phase [41]. The β-BeO phase is supposed to be a metastable state, which can be achieved by the application of low pressure (negative pressure) on wurtzite (B4) ZnO. Previously, Singh and Tripathi have investigated the β-BeO phase using the GGA method [42]. However, based on the literature review it is found that the structural, thermodynamic, and optoelectronic properties of β-BeO phase ZnO are still not studied in detail under varying decreasing pressure. The thermodynamic, structural, and optoelectronic properties of the β-BeO phase are significant in identifying the ZnO structure under pressure and designing various electronic devices [43–46].

Band gap plays an important role in the properties of materials, for example, a small band gap can cause the excellent electrical conductivity of thermoelectric materials [47, 48]. It is well-known that the wide band gap of materials can also result in extraordinary properties and application-oriented behaviour of materials. Therefore, tuning the band gap is a focus in both theoretical and experimental material sciences. First-principles method based on the density functional theory (DFT) technique, is a well-known computational method to explore the structural transition phenomena and properties of various materials [49–52]. However, first-principles with local density approximation (LDA) and generalized gradient approximation (GGA) computational methods cannot accurately estimate the band gap of metal oxide such as ZnO [53]. Furthermore, some researchers have found that the hybrid functional (Becke-Lee-Young-Parr exchange–correlation functional (B3LYP)) is an efficient approach to providing a reliable estimation of band gap and optical properties [54–57].

In this paper, based on the Debye model and first-principles method, we have systematically investigated the structural, thermodynamic, electronic, and optical properties of the recently predicted β-BeO phase of ZnO under variable negative pressure. First, the phase transition from B4 to β-BeO phase was found successfully by the LDA approximation. Then, the structural properties of the β-BeO phase were calculated to check its stability under different pressure conditions. The thermodynamic properties were calculated to investigate its thermodynamic permanence. Finally, the calculated electronic and optical properties demonstrated the nature of the β-BeO phase. Seemingly, this work introduces the β-BeO phase as a potential candidate material for developing nanostructured devices such as ZnO-based nanolasers in the chips tailored by pressure [58].

Moreover, the literature review has established that the ZnO from mineral inclusions provides information about the formation of minerals. Therefore, formation pressure can be determined based on this study [59].

Computational details

First-principles calculations were performed using Cambridge Sequential Total Energy Package (CASTEP) Program prompted in density functional theory (DFT) based on materials studio program [28, 60]. The procedures involved simulation, geometry optimization, and calculation of structural, electronic, and optical properties of B4 and β-BeO phase ZnO. The initial lattice parameters of the B4 phase take the experimental parameters and those of the BeO phase adopt the theoretical value [31, 33, 41]. After the stimulation of B4 and β-BeO type ZnO structures, we used the local density approximation (LDA) and Ceperley–Alder, and Perdew-Zunger method (CA-PZ) to get enthalpy [61]. Hydrostatic pressure is applied within the Parrinello–Rahman method [62]. The enthalpies we calculated were used to find the phase transformation pressure for the phase transition from B4 to β-BeO phase. The Monkhorst–Pack k points of $7 \times 7 \times 4$ for B4 phase and $4 \times 4 \times 7$ for the β-BeO phase were used for the first Brillouin zone sampling. The used displacement, stress, and maximum force are 0.002 Å, 0.1 GPa, and 0.05 eV/Å, respectively. The convergence energy was fixed at 2×10^{-5} eV/atom, and the cutoff energy was 500 eV. The electronic arrangement of Zn and O atoms in the B4 and β-BeO phases were $3d^{10}4s^2$ and $2s^22p^4$, respectively. We adopted the spin polarization, ultrasoft pseudopotentials [63], and Broyden-Fletcher-Goldfarb-Shanno (BFGS) algorithm [64] to handle electron–electron interactions. We found the total energy of B4 and β-BeO structures for different volumes by the LDA method, and then we plotted an energy-volume curve.

Becke three-parameter Lee–Yang–Parr functional (B3LYP) with separate X-C functional parameters [65], which is the hybrid correlation function, and the norm-conserving pseudopotentials were employed to evaluate the band structure and optical properties under controlling negative pressure. The applied value of X-C functional in this calculation was 0.4. The calculated band gap of B4 phase ZnO was 3.44 eV [66]; all observed properties match well with the experimental outcomes. This result confirms the reliability of the applied methodology and computational parameters. In these calculations, we used $4 \times 4 \times 2$ monkhorst-pack k points for B4 and $2 \times 2 \times 3$ for the β-BeO phase, and the cutoff energy was fixed at 1150.0 eV, which indicates that the plane wave in our calculations has kinetic energy ($\hbar^2k^2/2$ m) below 1150.0 eV. The cutoff energy we have taken can guarantee accuracy and convergence with limited computational resources. All calculations in this work were performed in reciprocal space.

The thermodynamic properties of B4 and β-BeO phase ZnO were estimated by employing the Debye model. Bulk modulus B was calculated by the Vinet equation of state (EOS) [67, 68]. Because the melting temperature of the wurtzite B4 ZnO is approximately 2248 K [69], we calculated the thermodynamic properties of B4 and β-BeO phase ZnO up to 2000 K. The value of thermal expansion coefficient (α) and heat capacity C_p are calculated by Eqs. (1) and (3).

$$\alpha(T) = \frac{1}{V(T)}\frac{\partial V(T)}{\partial T} \tag{1}$$

$$C_V = 3\mathrm{nk}\left[4D\left(\frac{\Theta}{T}\right) - \frac{3\Theta/T}{\exp\left(\Theta/T\right) - 1}\right] \tag{2}$$

$$C_p = C_v + \alpha^2\mathrm{BVT} \tag{3}$$

In Eq. 2, D denotes Debye integral and Θ symbolizes the temperature. The Θ, D, and $f(v)$ are calculated by Eqs. (4), (5), and (6). v is Poisson's ratio in Eq. (6).

$$\Theta = \frac{\hbar}{k_B}\left[6\pi^2V^{\frac{1}{2}}n\right]^{\frac{1}{3}}f(v)\sqrt{\frac{B}{M}} \tag{4}$$

$$D(y) = \frac{3}{y^3}\int_0^y \frac{x^3}{e^x - 1}dx \tag{5}$$

$$f(v) = \left\{3\left[2\left(\frac{2}{3}\frac{1+v}{1-2v}\right)^{\frac{3}{2}} + \left(\frac{1}{3}\frac{1+v}{1-v}\right)^{3/2}\right]^{-1}\right\}^{1/3} \tag{6}$$

where "M" and "n" are molecular mass per formula (81.38) and the number of atoms per unit cell (2) of ZnO in the β-BeO phase. The parameter "y" in Eq. 5 is Θ/T (Θ is Debye temperature). "x" in Eq. 5 is $\hbar\omega/k_BT$. "$\hbar$" is reduced Planck's constant or Dirac constant. "k_B" is the Boltzmann constant. The Poisson's ratio used in our calculation is 0.23 and 0.29 for β-BeO and B4 phases.

Results and discussion

Phase transitions, structural and thermodynamic properties

The pressure brought structural phase transition results in inducing unique optoelectronic properties in material structures. In this study, the transition of the wurtzite (B4) structure of ZnO to metastable β-BeO structure is achieved by decreasing pressure. Enthalpy (H) of B4 and β-BeO phase was calculated by doing geometry optimization under pressure range 0 ~ −18 GPa using the LDA method. The optimized structures of B4 and β-BeO type ZnO are displayed in Fig. 1. It is observed that enthalpies of B4 and β-BeO phases decrease with decreasing pressure. At the transition point, the enthalpy value of both phases became equal, and the structural phase transition is detected. The calculated transition graphs shown in Fig. 2 reveal that using the LDA method, the transition from B4 to β-BeO phase is found at −10.2 GPa. We also calculated the phonon dispersion of β-BeO phase ZnO and show it in Fig. 3. In Fig. 3 we can see that the phonon dispersion has positive and imaginary values under −15 and 0 GPa respectively, which means β-BeO phase ZnO is stable under −15 GPa. The result of phonon dispersion has the same conclusion with that of enthalpy shown in Fig. 2. The acquired transition pressure matches well with the predicted values reported by Zagorac et al. [41].

Structural properties play a significant role in persuading the electronic and optical behavior of materials. The calculated fundamental structural aspects of the B4 and β-BeO phases, such as crystal lattice parameters, bond angles, and bond lengths at 0 GPa and transition point −10.2 GPa, are listed in Table 1. The present calculation results are compared with previous structural data calculated by computational and experimental means. The trend of increasing lattice constants is observed with decreasing pressure. At 0 GPa, the lattice constants of β-BeO phase were $a = b = 5.451$ Å, $c = 3.215$ Å which later increased to $a = b = 5.666$ Å, $c = 3.244$ Å by applying the pressure −10.2 GPa. The cell volume increased from 23.892 Å at 0 GPa to 26.048 Å at −10.2 GPa. The bond length also firmly increases from 2.809 Å at 0 GPa to 2.877 Å at −10.2 GPa, ultimately influencing the hybridization of the Zn–O bond. Interestingly, the results have demonstrated that pressure has not affected the bond angle as its value $\alpha = \beta = \gamma = 90°$ is found the same at both 0 GPa and −10.2 GPa. Based on the enthalpy calculation shown in Fig. 2, it is found that the B4 phase possesses a low

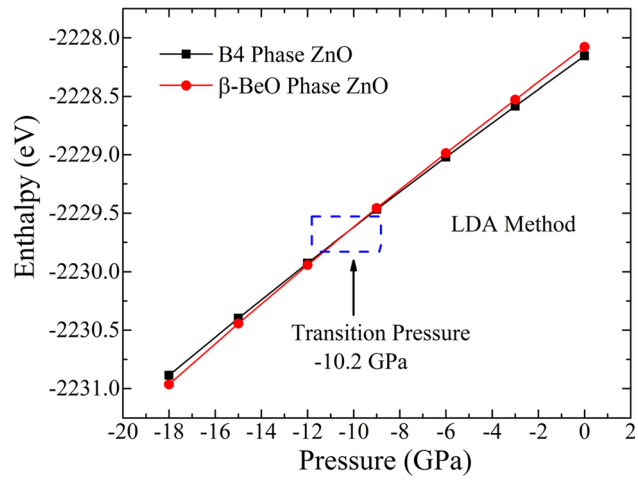

Figure 2 The enthalpy versus pressure graph for B4 and β-BeO phase. The cross point in the blue rectangle is the phase transition from B4 to β-BeO phase.

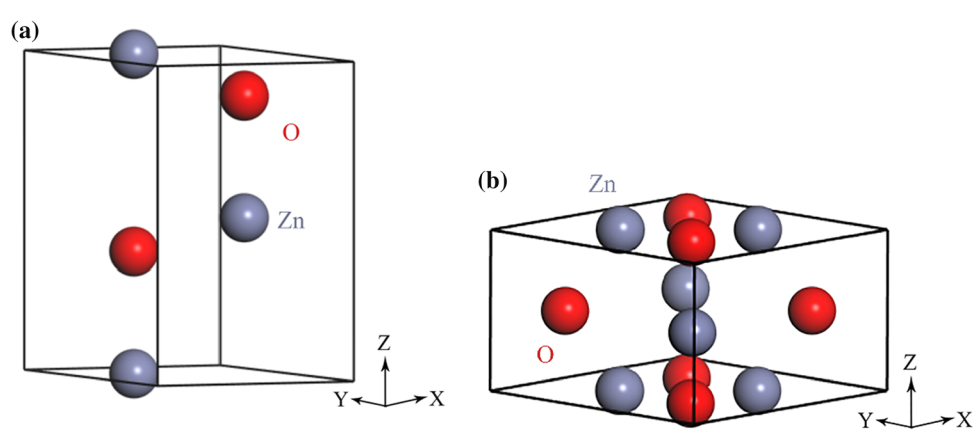

Figure 1 The optimized lattice structures of the B4 **a** and β-BeO phase **b** at 0 GPa. The red balls denote oxygen atoms and the gray ones specify zinc atoms in the crystal.

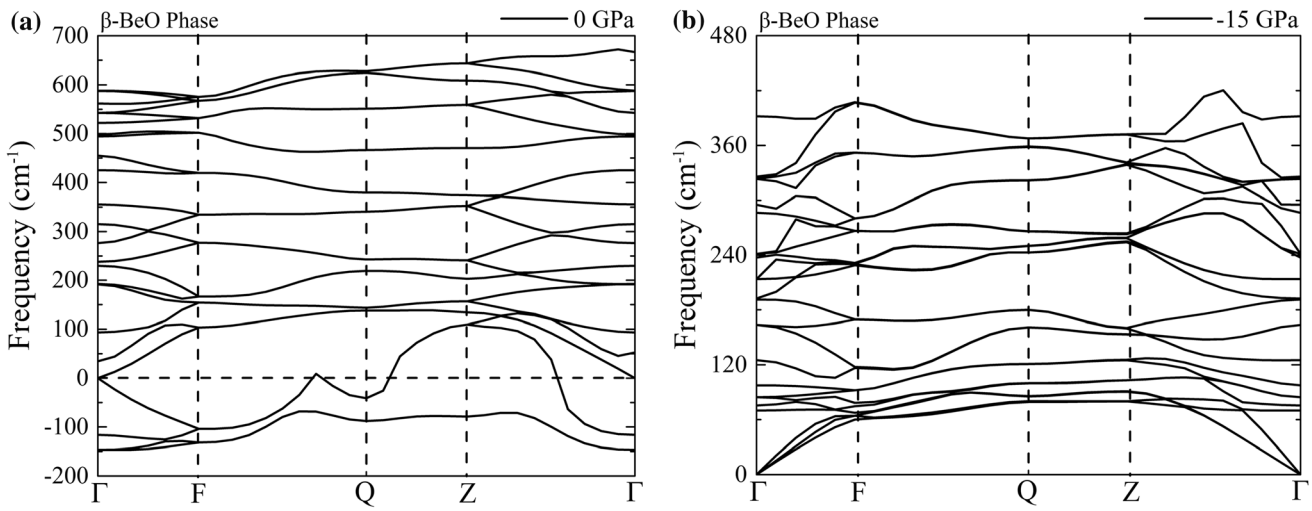

Figure 3 The calculated phonon dispersion for β-BeO phase ZnO under 0 and −15 GPa.

Table 1 The calculated lattice parameters, bond lengths, and volumes for B4 and β-BeO phase ZnO at 0 GPa and transition pressure −10.2 GPa. We compared our results with the previous theoretical and experimental results

Pressure (GPa)	Phase	Reference	$a = b$ (Å)	c (Å)	Bond Length (Å)	Volume (Å^3)
0	B4	Exp[a]	3.249	5.206		23.81
		Exp[b]	3.249	5.204		23.79
		Theory[c]	3.2562	5.2563	1.99	
		Theory[d]	3.209	5.128		22.80
		Theory[e]	3.19	5.18		
		Present	3.191	5.168	1.953	22.796
	BeO	Theory[e]	5.45	3.20		
		Present	5.451	3.215	2.809	23.892
−10.2	B4	Present	3.273	5.292	2.003	24.559
	BeO	Present	5.666	3.244	2.877	26.048

[a][31]
[b][33]
[c][38]
[d][39]
[e][41]

enthalpy value at "0" pressure and temperature conditions. It suggests that the B4 phase is the more stable phase.

The energy-volume relation was also determined, and the acquired results are plotted as a graph in Fig. 4. At equilibrium positions, the B4 and β-BeO phase ZnO possess low energy. Moreover, the graph shows that the minimum energy value calculated for the B4 phase is lower than the minimum energy value of the BeO phase. Hence, B4 is found to be a more stable phase. The point of intersection in the graph epitomizes that energy for the B4 and β-BeO phases are equal, and the structural phase transition begins after that point. The order of equilibrium energy, e.g., B4—β-BeO, evidenced the phase transition from B4 to β-BeO under pressure.

The thermodynamic properties under varying pressure are important for the practical applications of B4 and β-BeO phase ZnO. The calculated thermodynamic properties are shown in Fig. 4b–d, and our resulted values are in good agreement with the previous investigation reports of Seko et al. and Wu et al. [70, 71]. Figure 4b shows that the bulk modulus of B4 reduces with increasing the temperature or decreasing pressure. The determined bulk modulus value "B" of the β-BeO phase is lower than the B4 phase, which means the β-BeO phase is easier to compress than that of the B4 phase. Moreover, the bulk

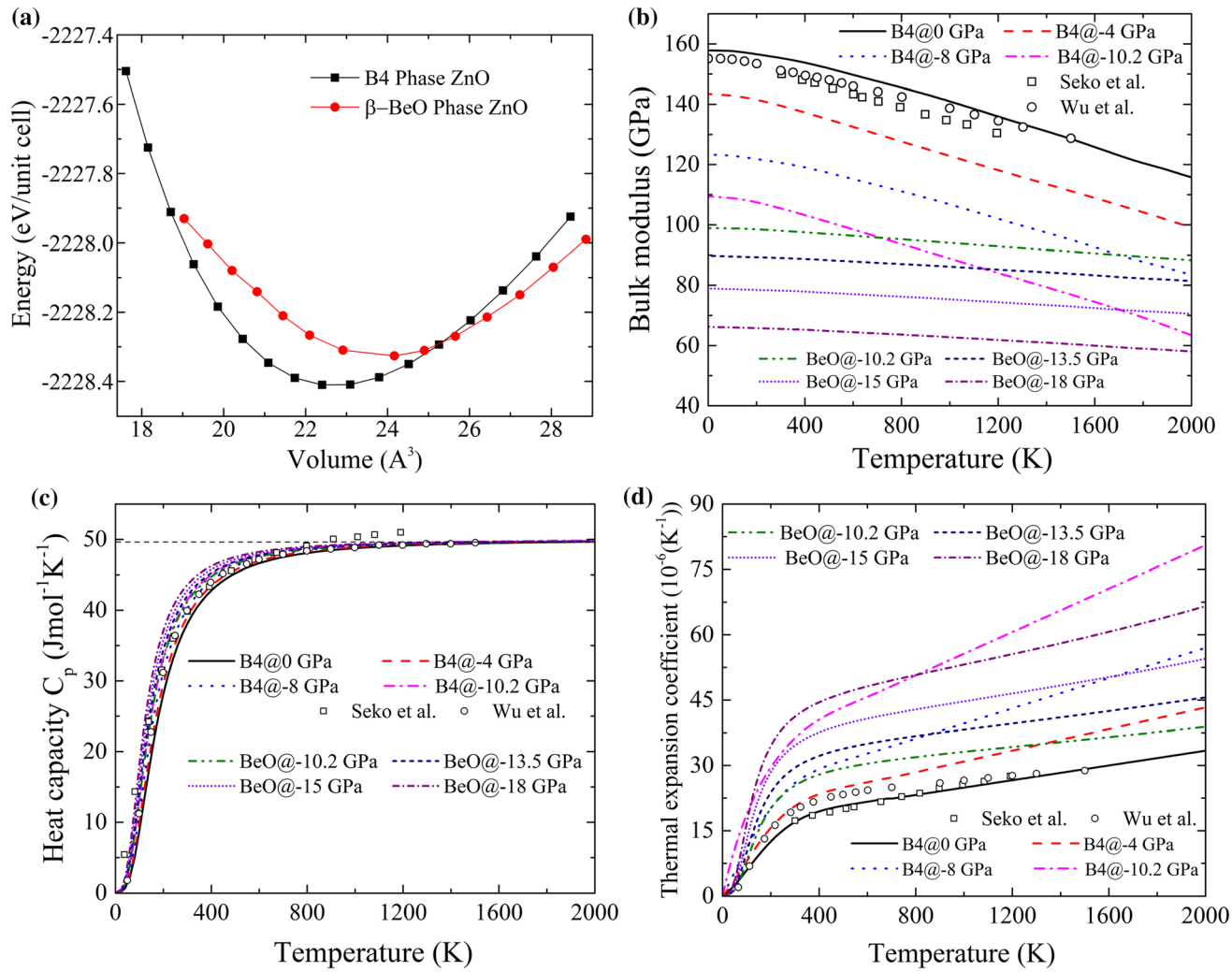

Figure 4 **a** Energy as a function of volume $E(V)$ graph for B4 and β-BeO phase of ZnO calculated at different fixed volumes, **b** The bulk modulus B, **c** heat capacity C_p, **d** thermal expansion coefficient (α) versus temperature and pressure.

modulus of the B4 phase decreases faster than the β-BeO phase, which can be used to detect the phase transformation. Figure 4c expresses that the value of C_p increases expeditiously before reaching a temperature of 246 K, and then its value became the Dulong-Peti limitation (49.7 $\text{Jmol}^{-1}\,\text{K}^{-1}$) around 700 K. The calculated thermal expansion coefficient α is shown in Fig. 4d. The α value rises with increasing temperature or decreasing pressure. It is found that the α increases fast below 220 K and slow above 220 K. With decreasing pressure, the α value also increases rapidly. At transition pressure and 0 K, the B, α, and C_p decreased compared to the B4 phase, which indicates the phase transition from B4 to β-BeO. These results also help to explain the change in B, α, and C_p aspects of materials under pressure in various geological processes. Additionally, the calculated thermodynamic properties can be used in developing various electronic devices.

Band gap and structure

Band gap and structure reveal the nature as well as electronic aspects of materials under applied pressure. Besides, these significant qualities also contribute to induce the transformation of excellent optical properties. To accurately examine the bands of optimized B4 and β-BeO phase ZnO structures, we used the hybrid functional (B3LYP) method. The calculated band structure of the B4 phase in the energy range $-10 \sim 25$ eV under varying negative pressure is given in Fig. 5a. The result shows that the valence band maximum (VBM) and conduction band

minimum (CBM) lie at same point (Γ–Γ). Hence it possesses a wider and direct band gap. The band gap is observed to decrease with decreasing the applied pressure. According to the results shown in Fig. 5c, the band gap of the B4 phase at 0 GPa is found 3.44 eV, and later it decreases to 3.34, 3.23, and 3.16 eV at −4, −8 GPa and transition pressure −10.2 GPa, respectively. We used a quadratic equation $E_g = 3.44 + 0.0227p - 4.64 \times 10^{-4}p^2$ to fit the band gap (eV) and pressure (GPa). The estimated band gap value and trend of decrease in band gap with decreasing pressure are found same as stated in the previous reports. The conduction band shifts to the upper energy level because of the improved repulsion in zinc (Zn) and oxygen (O) atoms. This atomic repulsion is linked to the change in bond and electronic cloud repulsion. Furthermore, the valence band is shifted to low energy because the Zn–O hybridization is enhanced.

We compared our calculated bandgap with other related reports (listed in Table 2). Our calculated band gap of B4 phase is 3.44 eV, which is found close to the previous experimental values (3.44 [66], 3.40 [5, 72], and 3.30 eV [73]). Moreover, this value 3.44 eV is also close to the previous theoretical results 3.761 [6], 3.21 [41] and 3.41 eV [74, 75]. Some researchers

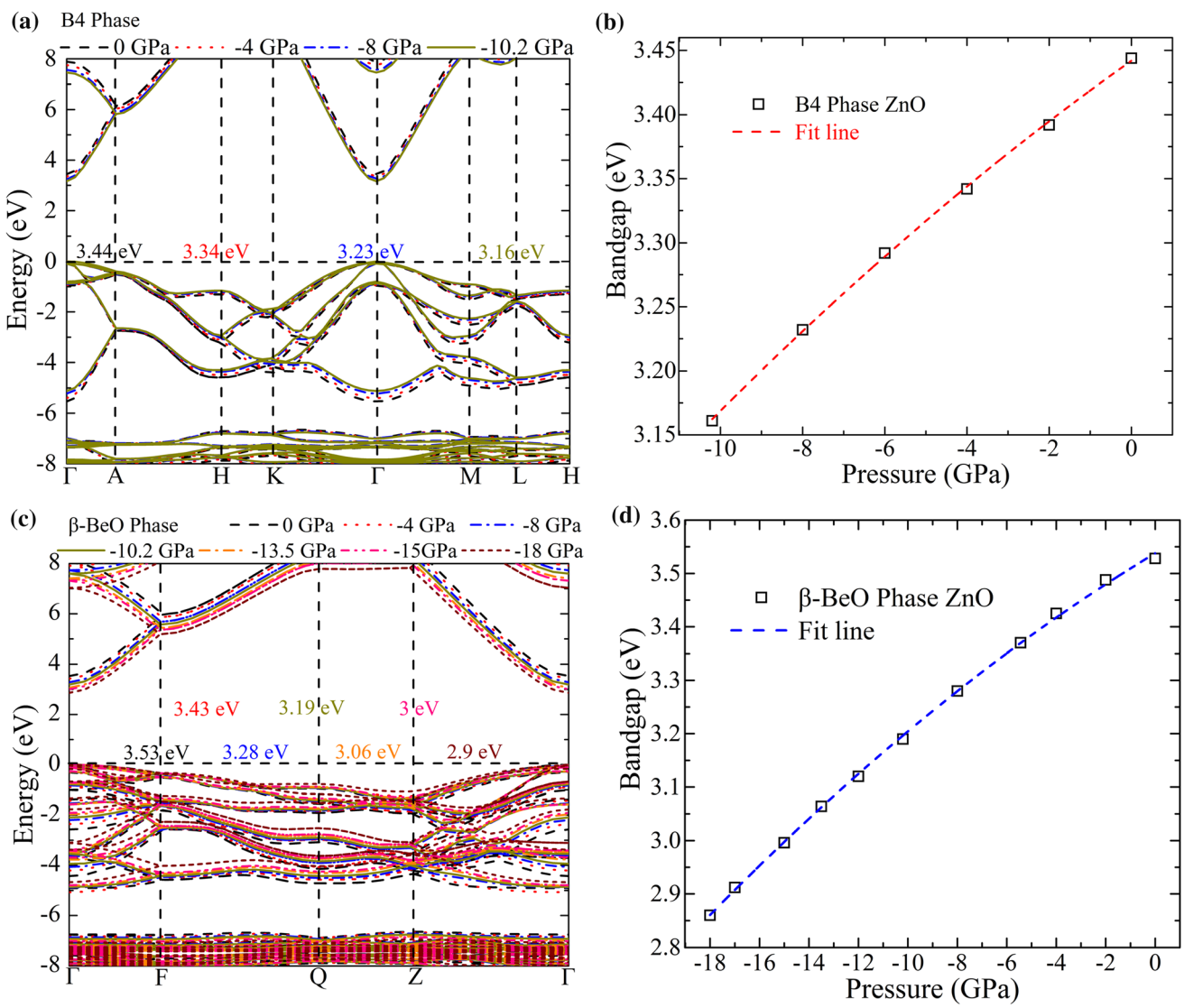

Figure 5 **a** The calculated band structure of B4 phase under 0 ∼ −10.2 GPa, **b** The estimated band gap values against pressure graph for B4 phase ZnO, **c** band structure of β-BeO phase at (0, −4, −8, −10.2, −13.5 and −18 GPa), **d** band gap versus pressure graph for β-BeO phase ZnO.

have found underestimated bandgap values (0.759, 0.830 [26] and 2.46 eV [76]) for B4 phase ZnO. This is because that these values were gotten using the usual first principles, which generally has the shortcoming of the underestimate band gap. Our calculated band gap is close to experimental values and major calculation results, which show that our results are reliable.

Bands calculation for β-BeO phase ZnO under negative pressure range 0 ~ −18 GPa shows significant results (Fig. 5b and d). At "0" GPa, the conduction band minimum and valence band maximum appear at the different points, so it is predicted to possess an indirect band gap. It is found that the β-BeO phase possesses large band gap energy of 3.53 eV. The large band gap expresses that the β-BeO phase is potentially active at a high temperature and in the ultraviolet region. For BeO phase ZnO, there are no experimental research for reference whereas previous computational investigations shown bandgap values 3.04 [25], 3.31, 1.31 eV [41], 2.85 [23], and 0.72 eV [77]. Our present calculated value 3.528 eV is greater than underestimated bandgap values and close to larger values. It is found that, with decreasing pressure, the band gap progressively decreases to 3.43, 3.28, 3.19, 3.06, 3.00 and 2.90 eV at −4, −8, −10.2, −13.5, −15 and −18 GPa, respectively.

Table 2 The calculated band gap (eV) for B4 and β-BeO phase ZnO under 0 GPa. We compared our results with the previous theoretical and experimental results

Phase	Theoretical	Experimental	Reference
B4	–	3.44	66
	–	3.40	5, 72
	–	3.30	73
	3.44	–	Present work
	3.761	–	6
	0.759	–	26
	0.830	–	26
	3.21	–	41
	3.41	–	74, 75
	2.46	–	76
BeO	3.528	–	Present work
	2.85	–	23
	3.04	–	25
	3.31	–	41
	0.72	–	77

In order of magnitude of energy dispersal, have made a clear analytical approach that the band gap steadily decreases with decreasing pressure. Hence, they are proportional to energy transformation. The narrowing band gap changes the electronic properties, which leads to the rise of a shift in the optical properties. The conduction band is shifted to a low energy level due to decreasing repulsion in Zn–O atoms. Simultaneously, the valence band is shifted to high energy due to the reduced Zn–O bond hybridization. A quadratic equation $E_g = 3.54 + 0.028p - 5.35 \times 10^{-4}p^2$ was used to fix the band gap, here E_g expresses energy (eV), and p represents the pressure in (GPa). The applied quadratic equation also helps to measure the pressure and detect the β-BeO phase of ZnO.

Electronic density of states

The electronic density of states is a key factor that determines the optical properties. We calculated the total density of states (DOS) and partial DOS (PDOS) to evaluate the contribution of different electronic states in inducing optical properties. The B4 phase is calculated under the pressure range 0 ~ −10.2 GPa, whereas the β-BeO phase is calculated under 0 ~ −18 GPa; the acquired results are plotted in Fig. 6. The Fermi level for this calculation was set as 0 eV. The lower value and upper value of the valence band for the B4 phase at 0 GPa and −10.2 GPa are differentiated through the energy −6.0 and −6.2 eV, respectively. It is observed that varying pressure has affected the hybridization. The resulting DOS is expended due to repulsion in the Zn–O bond.

Furthermore, the change of valence band to low energy and the conduction band to an upper energy level is observed critically. Hence the expansion in DOS, shifting of peaks, and variation in their shape clearly demonstrate the rise of interesting optical properties. We will discuss the relation of total DOS and partial DOS acquired for the β-BeO phase in detail as an example. The corresponding relation for the B4 phase can be understood in the same manner.

Figure 6b displays that for the β-BeO phase, the bands at 0 GPa and transition point −10.2 GPa are distinguished through the energy −5.2 and −5 eV. The valence band energy (−8.7 ~ 0 eV) at 0 GPa has resulted from two parts. The upper region (−5.2 ~ 0 eV) is linked to O 2p electronic state, and

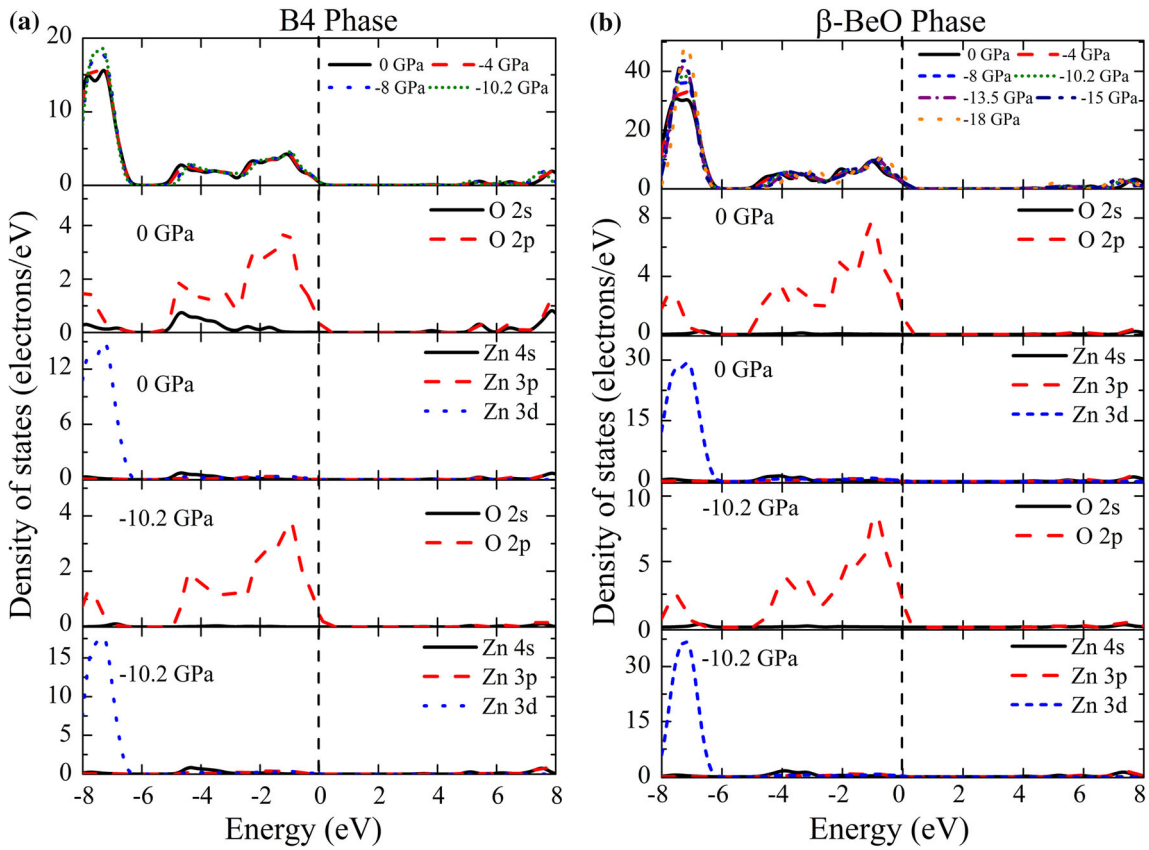

Figure 6 The calculated total and partial electronic density of states (DOS) of **a** B4 phase ZnO under 0 ~ −10.2 GPa, **b** β-BeO phase at (0 ~ −18 GPa). The vertical line at "0" shows the Fermi level between the valence and conduction band.

the lower region (−8.7 ~ −5.2 eV) originates from the Zn 3*d* electronic state. Additionally, the valence band energy (−19 ~ −17 eV) arises from the O 2*s* state, whereas the conduction band from O 2*s*, O 2*p*, Zn 4*s*, and Zn 3*p* electronic states. Furthermore, at transition pressure −10.2 GPa, the valence band −8.5 ~ 0 eV is separated by two regions. The region of energy −5 ~ 0 eV ascribes to the O 2*p* electronic state, whereas the energy range −8.5 ~ −5 eV to the Zn 3*d* state. Simultaneously, another valence band energy ranges in −18.5 ~ −16.5 eV attribute to the O 2*s* state. On the other hand, the conduction bands are produced due to the O 2*p*, Zn 4*s*, and Zn 3*p* electronic states. The strong hybridization of Zn 3*d* and O 2*p* states results in inducing the Zn–O bond, which conveys that ZnO possesses covalent nature.

Optical properties

The optical properties are interrelated to the electronic properties and give a better understanding of the electronic structure of the materials. The optical properties of the material also demonstrate its response to the incident electromagnetic radiation. Exploring the optical response of the material under different pressure is significant for its practical optoelectronic applications and develop various devices. To gain a deep insight into the optical response and electronic structure, we calculated the optical functions and optical constants such as dielectric function $\varepsilon(\omega)$, reflectivity $R(\omega)$, absorption $\alpha(\omega)$, the refractive index $n(\omega)$ and optical loss function $L(\omega)$. The properties of B4 phase ZnO are calculated at the pressure 0, −4, −8, and −10.2 GPa. Whereas for a detailed exploration, the properties of the β-BeO phase are calculated at pressure 0, −2, −4, −6, −8, −10.2, −13.5, −15, and −18 GPa. The optical constants calculations are under 0 K.

Dielectric function

The complex dielectric function $\varepsilon(\omega)$ describes the optical response of the material to electromagnetic radiation. It consists of real and imaginary parts:

$\varepsilon(\omega) = \varepsilon_1(\omega) + i\varepsilon_2(\omega)$. The real part $\varepsilon_1(\omega)$ characterizes the photon dispersion, and it can be calculated using Kramer's-Kronig relation. On the other hand, the imaginary part $\varepsilon_2(\omega)$ describes the photon absorption induced due to the electronic transition between occupied and unoccupied states. It can be calculated by momentum matrix elements between the occupied and unoccupied states in electronic wave functions. The dielectric function is also significant in determining other optical constants. In this work, the dielectric function was calculated to investigate the pressure-induced optical changes in B4 and β-BeO phase ZnO.

The imaginary part of dielectric function $\varepsilon_2(\omega)$ is calculated using the equation

$$\varepsilon_2(\omega) = \frac{2e^2\pi}{\varepsilon_0} k, v, c \, \Psi_k^c \hat{u} \cdot r \Psi_k^v (E_k^c - E_k^v - E) \tag{7}$$

In this equation, ω represents the frequency of incident photons through the crystal. The Ω denotes unit cell volume, ε_0 is the permittivity in free space, and k is the reciprocal lattice vector. The superscripts c and v represent the conduction and valence bands.

The real part of dielectric function $\varepsilon_1(\omega)$ is calculated by the Kramer's-Kronig equation

$$\varepsilon_1(\omega) = 1 + \frac{2}{\pi} \mathrm{P} \int_0^\infty \frac{\omega' \varepsilon_2(\omega')}{\omega'^2 - \omega^2} d\omega' \tag{8}$$

The function P is the principal value.

Figure 7 depicts the calculated imaginary part $\varepsilon_2(\omega)$ for B4 and β-BeO phase ZnO under the photon energy range 0 to 55 eV. As shown in Fig. 7a, the starting energy for the B4 phase at 0 and transition pressure −10.2 GPa is 2.2 and 1.9 eV, respectively. At −10.2 GPa, the prominent peaks are found at 3.6, 5.4, and 8.5 eV. These peaks are originated mainly due to optical transition between the maximum of the valence band and the minimum of the conduction band. Additionally, the extreme peak found at 15 eV is arising due to the strong transition to the unoccupied orbital in the conduction band. Figure 7b displays the calculated $\varepsilon_2(\omega)$ results for the β-BeO phase. The starting energy at 0 and transition pressure −10.2 GPa are 2.7 and 2.4 eV, respectively. It is seen that the β-BeO phase profile is contracted in value compared to the B4 phase between 4 and 42 eV. The contraction in the profile is associated with the contraction in the corresponding DOS. It specifies that the β-BeO phase has extraordinary properties in the ultraviolet region of energy. The resulted graph also shows that the β-BeO phase has a prominent decreased peak (8.1 eV) at −10.2 GPa, indicating the transition of B4 to the β-BeO phase. The maximum $\varepsilon_2(\omega)$ peak is found at 14 eV. The profile change and redshift are accredited to the decreased band gap, i.e., 3.53 ∼ 3.19 eV. The peaks around 5 eV come from O 2p to Zn 4s transition. The peak at 8.1 eV is originated from Zn 3d to O 2p states. The peak around 14 eV comes from Zn 3d to O 2s state transition [78].

The real part of the dielectric function $\varepsilon_1(\omega)$ is the key feature for demonstrating the optoelectronic applications of the β-BeO phase under pressure. According to the calculated results shown in Fig. 7c, the starting $\varepsilon_1(\omega)$ for the B4 phase at 0 GPa is 2.70 eV, whereas 2.75 eV at −10.2 GPa. The $\varepsilon_1(\omega)$ of the B4 phase changes slowly and almost keeps a similar shape below 2.5 eV. Some $\varepsilon_1(\omega)$ peaks are found to fall in the negative region at around 17.1 eV. Figure 7d shows that the starting $\varepsilon_1(\omega)$ of β-BeO phase at 0 GPa is 2.58 eV, whereas 2.62 eV at transition pressure −10.2 GPa. The β-BeO phase keeps an almost constant $\varepsilon_1(\omega)$ value below 2.5 eV. These results express that the effect of pressure is minute in the low-energy region. According to the profile of $\varepsilon_1(\omega)$, the β-BeO phase possesses dielectric nature in the visible energy region. Furthermore, at −10.2 GPa, the $\varepsilon_1(\omega)$ starting energy value 2.73 eV for the B4 phase is shifted to 2.62 eV for the β-BeO phase. This redshift (decrease in energy) identifies the transition of the B4 structure to the β-BeO structure. On the other hasnd, some $\varepsilon_1(\omega)$ peaks fall in the negative range. It reveals the changing dielectric nature of the material to a metallic behavior and is noted for practical applications. The metallic nature represents that the material contains a large number of carriers, whereas the dielectric nature indicates a small number of carriers. The β-BeO phase shows metallic nature at about 16.3 eV. Generally, the dielectric function calculations have demonstrated that the β-BeO phase shows diverse properties and behavior below the 50 eV. The acquired results are substantial in expressing the applications of the β-BeO phase for manufacturing electronic devices in future.

Optical constants

The absorption coefficient ($\alpha(\omega)$), reflectivity ($R(\omega)$), loss function ($L(\omega)$), and real part of the refractive index ($n(\omega)$) are key optical constants in determining the optical response of a material to the incident light.

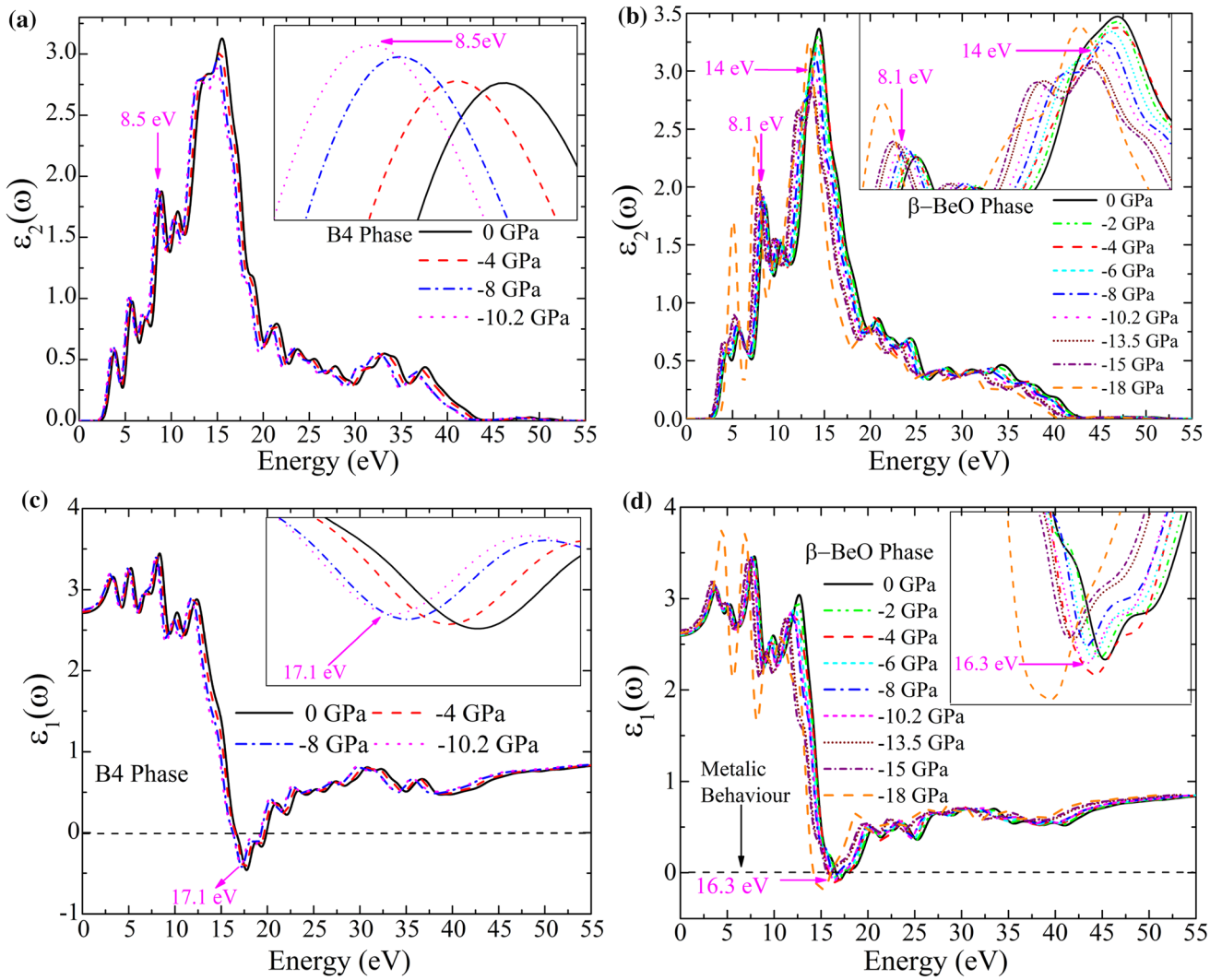

Figure 7 The calculated imaginary part $\varepsilon_2(\omega)$ **a**, **b** and real part $\varepsilon_1(\omega)$ **c**, **d** of the dielectric function for B4 and real for B4 ($0 \sim -10.2$ GPa) and β-BeO phase ($0 \sim -18$ GPa).

These functions also identify the potential and significant properties of the materials for their applications in optoelectronic devices. Optical constants can be calculated by using the following equations, which include the dielectric function.

$$\alpha(\omega) = \sqrt{2\omega}\left[\sqrt{\varepsilon_1^2(\omega) + \varepsilon_2^2(\omega)} - \varepsilon_1(\omega)\right]^{1/2} \tag{9}$$

$$R(\omega) = \left|\frac{\sqrt{\varepsilon_1(\omega) + i\varepsilon_2(\omega)} - 1}{\sqrt{\varepsilon_1(\omega) + i\varepsilon_2(\omega)} + 1}\right|^2 \tag{10}$$

$$n(\omega) = \left[\sqrt{\varepsilon_1^2(\omega) + \varepsilon_2^2(\omega)} + \varepsilon_1(\omega)\right]^{1/2} / \sqrt{2} \tag{11}$$

$$L(\omega) = \frac{\varepsilon_2(\omega)}{\varepsilon_1^2(\omega) + \varepsilon_2^2(\omega)} \tag{12}$$

The calculated optical constants result for B4 and β-BeO phase under $0 \sim 55$ eV photon energy are presented in Figs. 8 and 9. Figure 8a illustrates that absorption coefficient $\alpha(\omega)$ for the B4 phase under transition pressure -10.2 GPa has a prominent peak at 8.7 eV. The results given in Fig. 8b show that the $\alpha(\omega)$ of the β-BeO phase possesses a wide energy region, which expresses its extensive applications. It is observed that the absorption value of the β-BeO phase is zero in the infrared and visible regions. With decreasing pressure, the β-BeO phase undergoes a redshift in the peak values. The Peak values decreased compared to the peak values of the B4

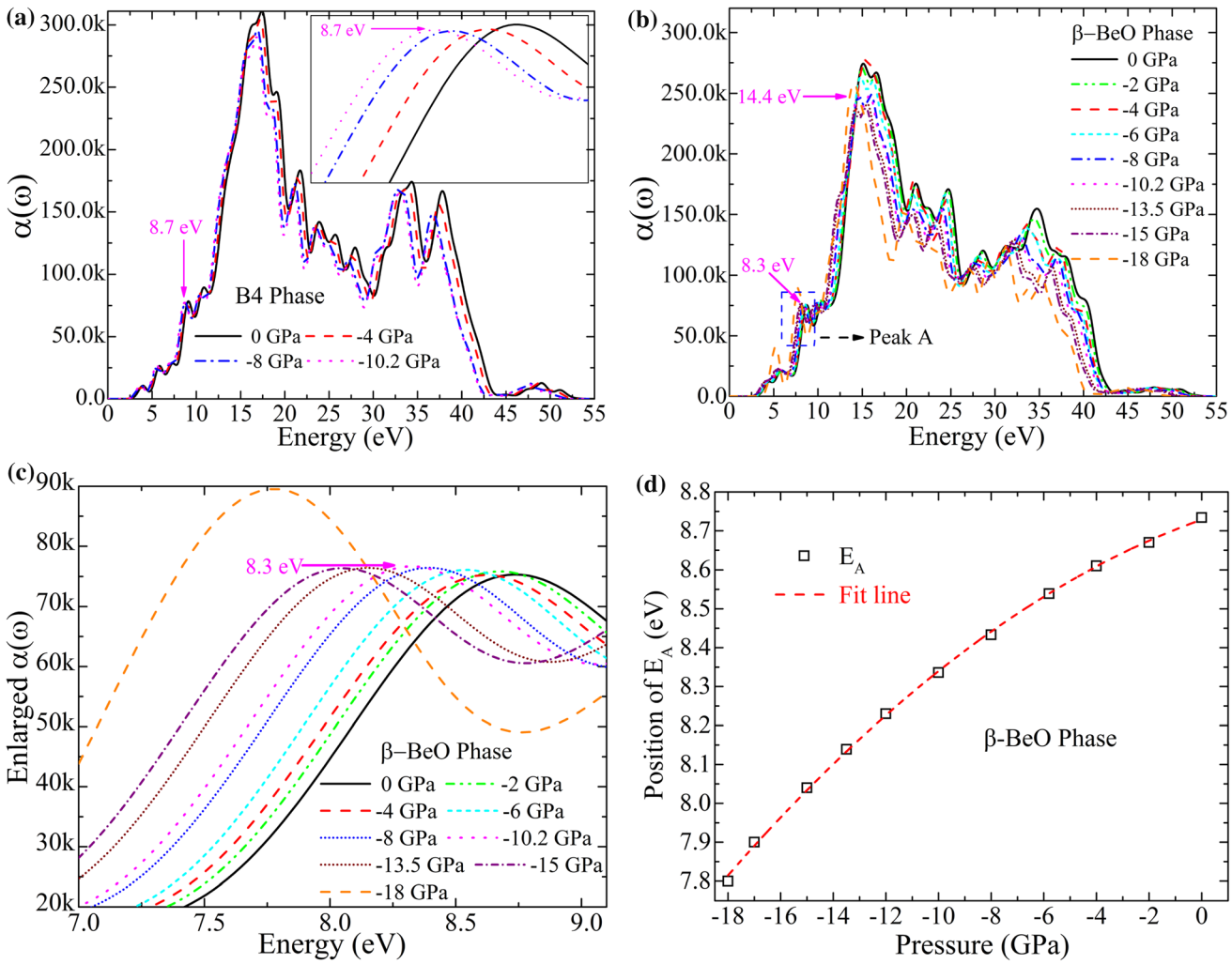

Figure 8 The absorption coefficient $\alpha(\omega)$ of **a** B4 and **b** β-BeO phase ZnO, **c** enlarged view of absorption for β-BeO phase under pressure $0 \sim -18$ GPa, **d** position of E_A versus pressure graph.

phase. At −10.2 GPa, the decreased peak of the β-BeO phase (8.3 eV) epitomizes the phase transformation from B4 to the β-BeO phase. The redshift of $\alpha(\omega)$ peaks with decreasing pressure is important in identifying phase transition and determining the pressure after standardization. The redshift is associated with the decrease in the band gap and the corresponding change in the DOS. The peak of $\alpha(\omega)$ lies in the ultraviolet energy range. It shows that the β-BeO phase is a promising material for photon absorption in the ultraviolet region. The maximum absorption peak is found at 14.4 eV. We selected a peak "A" of the β-BeO phase to better analyze and specify the phase transition. The relation between changing positions of peak E_A and rising pressure for optical constant $\alpha(\omega)$ is discussed as an example. The relation for other optical constants can be understood in the same manner. The extended image of absorption peak "A" for the β-BeO phase under pressure is given in Fig. 8c. It shows the gradual decrease in the peak position with decreasing pressure under $0 \sim -18$ GPa. The relation between the position of peak E_A and pressure is expressed in Fig. 8d. A quadratic equation $E_A = 8.729 + 0.0241p - 0.00148p^2$ was used to adjust the relation. The E_A is taken in the unit eV, whereas the p is taken in GPa.

The reflectivity $R(\omega)$ is a ratio between the energies of reflected and incident waves from the material's surface. The reflectivity $R(\omega)$ profile against photon energy (eV) under pressure is plotted in Fig. 9. It is observed that the $R(\omega)$ values for B4 and β-BeO phase are nearly constant in the infrared region below 1.7 eV. At −10.2 GPa, the B4 phase has a prominent peak at 8.3 eV. The maximum $R(\omega)$ peaks for the B4

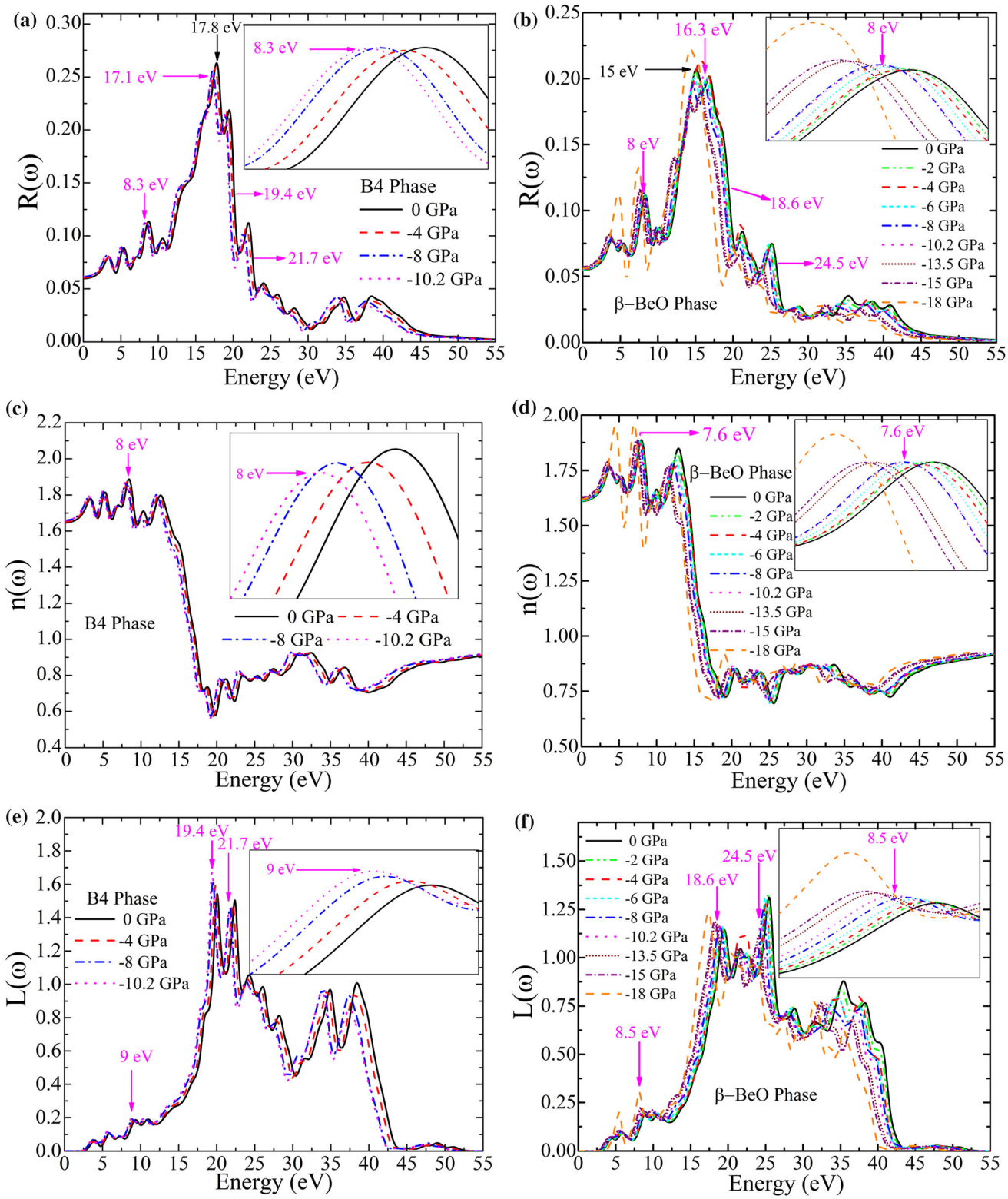

Figure 9 The reflectivity $R(\omega)$ **a**, **b**, real part of refractive index $n(\omega)$ **c**, **d** and estimated loss function $L(\omega)$ **e**, **f** results for B4 and β-BeO phase under 0 $\sim$ -10.2 and 0 $\sim$ -18 GPa.

phase at about 17.8 and 17.1 eV under 0 and −10.2 GPa, respectively. The maximum ratio of the reflectivity calculated for the B4 phase is 26 %. Additionally, the $R(\omega)$ of the B4 phase has a peak drop at 19.4 and 21.7 eV. Figure 9b shows that the peak position of the β-BeO phase decreased to 8 eV compared with that of the B4 phase, which epitomizes the transition of B4 to the β-BeO phase. The maximum $R(\omega)$ peaks for β-BeO phase are found in the ultraviolet region at about 15 eV (@0 GPa) and 16.3 eV (@−10.2 GPa). The acquired maximum $R(\omega)$ corresponds to the negative real part of the dielectric function $\varepsilon_1(\omega)$. The maximum ratio of calculated reflectivity for the β-BeO phase is 20 %. These results demonstrate that the β-BeO phase exhibits a lower ratio of the incident light than the B4 phase. The $R(\omega)$ of the β-BeO phase has undergone a peak drop phenomenon at 18.6 and 24.5 eV, which corresponds to the maximum peaks produced for the loss function $L(\omega)$. The peak drop points match well with the extreme peak values of $L(\omega)$. The reflectivity is observed to become almost zero for energies greater than 50 eV.

The refractive index $n(\omega)$ of a material defines how a photon propagates through the medium and determines its phase velocity. It also evaluates the material's optically dispersed behavior, so it is essential for photonic applications such as optical waveguides. The calculated refractive index $n(\omega)$ for B4 and β-BeO phase are presented by plotting a graph in Fig. 9c and d. It is observed that the $n(\omega)$ profile for considering phases resembles the profile of $\varepsilon_1(\omega)$ under the same pressure range. For the B4 phase at −10.2 GPa, the $n(\omega)$ starts at 1.65 eV and gradually increases below 11.9 eV. Simultaneously, the $n(\omega)$ for the β-BeO phase originates at 1.6 eV and rises smoothly. The B4 and β-BeO phase exhibits an almost similar profile shape except for the minor difference in starting values. The B4 phase possesses a prominent peak at 8 eV while the β-BeO phase undergoes redshift and its peak value (7.6 eV) is less than the B4 phase. The redshift in the peak value indicates the phase transition. After 12.2 eV, a steady peak drop in the $n(\omega)$ profile is critically observed. The steady peak drop in $n(\omega)$ is noteworthy for practical applications of β-BeO phases.

The loss function $L(\omega)$ is an essential feature that describes the energy loss by the electron when it is traversed in a crystal material. Figure 9e and f shows the graphical results of $L(\omega)$ for B4 and β-BeO phase ZnO. The $L(\omega)$ peaks almost uniformly increase under the energy range 2.2 to 15 eV, then increase abruptly beyond this point. At −10.2 GPa, the B4 phase has a prominent peak at 9 eV, whereas the β-BeO phase has a decreased peak value (8.5 eV), which specifies the phase transition. The main peaks in the $L(\omega)$ graph refer to plasma resonance, and their frequency is called plasma frequency. The maximum $L(\omega)$ peaks of the B4 phase at 19.4 and 21.7 eV are in accordance with the declining peaks of reflectivity $R(\omega)$. Simultaneously, the maximum $L(\omega)$ peak values (18.6 and 24.5 eV) of the β-BeO phase also match well with the declined peak positions of $R(\omega)$. It is observed that both B4 and β-BeO phase has almost the same expansion of the profile between 2.7–52 eV. The loss in energy $L(\omega)$ is nearly zero beyond 52 eV. It is found that under the visible energy region (1.61–3.10 eV), the initial energy results of $\alpha(\omega)$, $L(\omega)$, and $n(\omega)$ are observed 0, 0, and 1.60. These significant optical results express that the β-BeO phase exhibits a transparent material nature.

Conclusions

In this work, the phase transition, thermodynamic, structural, electronic, and optical properties of β-BeO phase ZnO were investigated under negative pressure. The enthalpy calculation has revealed the structural phase transition from wurtzite B4 to β-BeO phase occurred at −10.2 GPa. The calculated transition pressure value and lattice parameters are in fairly good agreement with the previous reports. The thermodynamic quantities undergo a decrease in values at the phase transition point. Band structure analyses show that the β-BeO phase possesses a wider indirect band gap, which progressively decreases with decreasing pressure. It has been found that optical properties undergo a redshift with decreasing the pressure. The optical properties results have demonstrated the dielectric, metallic and transparent nature of the β-BeO phase under varying pressure. This investigation is a profound source to verify the existence of the metastable β-BeO phase in the ZnO system and its experimental exploration in future. Moreover, it paves a feasible way for the practical applications of the β-BeO phase in developing various ZnO-based nanostructured electronic devices.

Acknowledgements

The project was supported by the National Key Research and Development Project (No. 2018YFA0702702), National Natural Science Foundation of China (Nos. 42072050 and 41402034), China Postdoctoral Science Foundation (Nos. 2018T110815 and 2016M600622) and the Fundamental Research Funds for the Central Universities, China University of Geosciences (Wuhan) (CUGL150418), Foundation of Cultivation of Scientific Institutions of Jianghan University.

Declarations

Conflict of interest The authors declare that they have no conflict of interest.

References

[1] Long X, Qiu W, Wang Z, Wang Y, Yang S (2019) Recent advances in transition metal–based catalysts with heterointerfaces for energy conversion and storage. Mater Today Chem 11:16–28. https://doi.org/10.1016/j.mtchem.2018.09.003

[2] Xue Y, Zhang Q, Wang W, Cao H, Yang Q, Fu L (2017) Opening two-dimensional materials for energy conversion and storage: a concept. Adv Energy Mater 7:1602684. https://doi.org/10.1002/aenm.201602684

[3] Zhao K, Qiu P, Shi X, Chen L (2020) Recent advances in liquid-like thermoelectric materials. Adv Funct Mater 30:1903867. https://doi.org/10.1002/adfm.201903867

[4] Harun K, Salleh NA, Deghfel B, Yaakob MK, Mohamad AA (2020) DFT + U calculations for electronic, structural, and optical properties of ZnO wurtzite structure: a review. Results Phys 16:102829. https://doi.org/10.1016/j.rinp.2019.102829

[5] Özgür Ü, Alivov YI, Liu C, Teke A, Reshchikov MA, Doğan S, Avrutin V, Cho SJ, Morkoç H (2005) A comprehensive review of ZnO materials and devices. J Appl Phys 98:041301. https://doi.org/10.1063/1.1992666

[6] Wang J, Shen T, Feng Y, Liu H (2020) A GGA+U study of electronic structure and the optical properties of different concentrations Tb doped ZnO. Physica B 576:411720. https://doi.org/10.1016/j.physb.2019.411720

[7] Klingshirn C, Fallert J, Zhou H, Sartor J, Thiele C, Maier-Flaig F, Schneider D, Kalt H (2010) 65 years of ZnO research-old and very recent results. Phys Status Solidi (B) 247:1424–1447. https://doi.org/10.1002/pssb.200983195

[8] Wang Z, Wang H, Wang L, Zhao H, Kamboh MA, Hao L, Chen Q, He K, Wang Q (2020) Influence of Cu dopant on the electronic and optical properties of graphene-like ZnO monolayer. Physica E 115:113702. https://doi.org/10.1016/j.physe.2019.113702

[9] Wang L, Wu J, Shang MH, Gao FM, Li XX, Zheng YP, Zhang DD, Yang WY, Chen SL (2021) Improved piezoresistive properties of ZnO/SiC nanowire heterojunctions with an optimized piezoelectric nanolayer. J Mater Sci 56(2021):17146–17155. https://doi.org/10.1007/s10853-021-06411-1

[10] Koutavarapu R, Manepalli RKNR, Madhav BTP, Satyanarayana T, Nagarjuna G, Shim J, Rao MC (2020) Optical, electrical and photoluminescence studies on Al_2O_3 doped PVA capped ZnO nanoparticles for optoelectronic device application. Optik 205:164236. https://doi.org/10.1016/j.ijleo.2020.164236

[11] Otalora C, Botero MA, Ordonez G (2021) ZnO compact layers used in third-generation photovoltaic devices: a review. J Mater Sci 56:15538–15571. https://doi.org/10.1007/s10853-021-06275-5

[12] Pei J, Feng K, Zhao X, Hao Y, Wei Y, Chen S, Sun B, Li Y, Lv H (2019) ZnO-based inverted hybrid solar cells using P3HT and spiro-OMeTAD with hole transporting property: layered or blended. Chem Phys Lett 729:79–83. https://doi.org/10.1016/j.cplett.2019.05.021

[13] Saleh Al-Khazali SM, Al-Salman HS, Hmood A (2020) Low cost flexible ultraviolet photodetector based on ZnO nanorods prepared using chemical bath deposition. Mater Lett 277:128177. https://doi.org/10.1016/j.matlet.2020.128177

[14] Ppong SOB, Opoku F, Anku WW, Govender PP (2021) Insights into the complementary behaviour of Gd doping in GO/Gd/ZnO composites as an efficient candidate towards photocatalytic degradation of indigo carmine dye. J Mater Sci 56:8511–8527. https://doi.org/10.1007/s10853-021-05846-w

[15] Kim HT, Lee SY, Slaoui A, Dinia A, Jeon HJ, Park C (2021) Properties of Yb-added ZnO (Yb:ZnO) films as an energy-conversion layer on polycrystalline silicon solar cells. Mater Chem Phys 265:124513. https://doi.org/10.1016/j.matchemphys.2021.124513

[16] Fahimi Z, Moradlou O (2020) Fabrication of ZnO@C foam: a flexible free-standing electrode for energy storage devices. Mater Design 189:108525. https://doi.org/10.1016/j.matdes.2020.108525

[17] Kaminsky F (2012) Mineralogy of the lower mantle: A review of 'super-deep' mineral inclusions in diamond. Earth Sci Rev 110:127–147. https://doi.org/10.1016/j.earscirev.2011.10.005

[18] Ul Haq B (2021) First-principles calculations to investigate thermoelectric properties of new monolayers of ZnO. Optik 238:166782. https://doi.org/10.1016/j.ijleo.2021.166782

[19] Gahlan HA, Arai S, Ahmed AH, Ishida Y, Abdel-Aziz YM, Rahimi A (2006) Origin of magnetite veins in serpentinite from the Late Proterozoic Bou-Azzer ophiolite, Anti-Atlas, Morocco: an implication for mobility of iron during serpentinization. J Afr Earth Sci 46:318–330. https://doi.org/10.1016/j.jafrearsci.2006.06.003

[20] Hattabi I, Abdiche A, Semari F, Khenata R, Soyalp F (2018) Pressure effect on the structural, electronic and optical properties of the cubic triangular quaternary $BN_xAs_yP_{1-x-y}$ alloys: first principle study. Chinese J Phys 56:2332–2349. https://doi.org/10.1016/j.cjph.2018.06.025

[21] Haq BU, Afaq A, Ahmed R, Naseem S (2012) A comprehensive DFT study of zinc oxide in different phases. Int J Mod Phys C 23:1250043. https://doi.org/10.1142/s012918311250043x

[22] Ul Haq B, AlFaify S, Alrebdi TA, Ahmed R, Al-Qaisi S, Taib MFM, Naz G, Zahra S (2021) Investigations of optoelectronic properties of novel ZnO monolayers: a first-principles study. Mater Sci Eng B 265:115043. https://doi.org/10.1016/j.mseb.2021.115043

[23] Shabbir S, Shaari A, Ul Haq B, Ahmed R, AlFaify S, Ahmed M, Laref A (2020) First-principles investigations of structural parameters, electronic structures and optical spectra of 5–5-and BeO-type of $ZnO_{1-x}S_x$ alloys. Mater Sci Eng B 262:114697. https://doi.org/10.1016/j.mseb.2020.114697

[24] Bakhtiar UH, Ahmed R, Khenata R, Ahmed M, Hussain R (2013) A first-principles comparative study of exchange and correlation potentials for ZnO. Mater Sci Semicond Process 16:1162–1169. https://doi.org/10.1016/j.mssp.2012.11.012

[25] Shabbir S, Shaari A, Ul Haq B, Alfaify S, Ahmed R, Ahmed M (2021) Exploring the thermoelectric response of novel polymorphs of ZnO for renewable energy applications using first-principles approaches. Optoelectron Adv Mat 15:286–293

[26] Ul Haq B, Ahmed R, Goumri-Said S, Shaari A, Afaq A (2013) Electronic structure engineering of ZnO with the modified Becke-Johnson exchange versus the classical correlation potential approaches. Phase Trans 86:1167–1177. https://doi.org/10.1080/01411594.2012.755183

[27] Ul Haq B, AlFaify S, Alshahrani T, Ahmed R, Butt FK, Rehman SU, Tariq Z (2020) Devising square- and hexagonal-shaped monolayers of ZnO for nanoscale electronic and optoelectronic applications. Sol Energy 211:920–927. https://doi.org/10.1016/j.solener.2020.09.075

[28] Segall MD, Lindan PJD, Probert MJ, Pickard CJ, Hasnip PJ, Clark SJ, Payne MC (2002) First-principles simulation: ideas, illustrations and the CASTEP code. J Phys 14:2717–2744. https://doi.org/10.1088/0953-8984/14/11/301

[29] Burke K (2012) Perspective on density functional theory. J Chem Phys 136:150901. https://doi.org/10.1063/1.4704546

[30] Liebermann RC (2011) Multi-anvil, high pressure apparatus: a half-century of development and progress. High Pressure Res 31:493–532. https://doi.org/10.1080/08957959.2011.618698

[31] Desgreniers S (1998) High-density phases of ZnO: Structural and compressive parameters. Phys Rev B 58:14102–14105. https://doi.org/10.1103/PhysRevB.58.14102

[32] Liu H, Tse JS, Mao HK (2006) Stability of rocksalt phase of zinc oxide under strong compression: synchrotron x-ray diffraction experiments and first-principles calculation studies. J Appl Phys 100:093509. https://doi.org/10.1063/1.2357644

[33] Karzel H, Potzel W, Köfferlein M, Schiessl W, Steiner M, Hiller U, Kalvius GM, Mitchell DW, Das TP, Blaha P, Schwarz K, Pasternak MP (1996) Lattice dynamics and hyperfine interactions in ZnO and ZnSe at high external pressures. Phys Rev B 53:11425–11438. https://doi.org/10.1103/PhysRevB.53.11425

[34] Amrani B, Chiboub I, Hiadsi S, Benmessabih T, Hamdadou N (2006) Structural and electronic properties of ZnO under high pressures. Solid State Commun 137:395–399. https://doi.org/10.1016/j.ssc.2005.12.020

[35] Jaffe JE, Snyder JA, Lin Z, Hess AC (2000) LDA and GGA calculations for high-pressure phase transitions in ZnO and MgO. Phys Rev B 62:1660–1665. https://doi.org/10.1103/PhysRevB.62.1660

[36] Cui S, Feng W, Hu H, Feng Z, Wang Y (2009) Structural and electronic properties of ZnO under high pressure. J Alloys Compd 476:306–310. https://doi.org/10.1016/j.jallcom.2008.08.052

[37] Zhang FY (2011) A possible new transition path for ZnO from B4 to B1. Physica B 406:3942–3946. https://doi.org/10.1016/j.physb.2011.07.032

[38] Pu CY, Tang X, Zhang QY (2011) First principles study on the structural and optical properties of the high-pressure ZnO phases. Solid State Commun 151:1533–1536. https://doi.org/10.1016/j.ssc.2011.07.034

[39] Molepo MP, Joubert DP (2011) Computational study of the structural phases of ZnO. Phys Rev B 84:094110. https://doi.org/10.1103/PhysRevB.84.094110

[40] Li Z, Xu Y, Gao G, Cui T, Ma Y (2009) Tetragonal high-pressure phase of ZnO predicted from first principles. Phys Rev B 79:193201. https://doi.org/10.1103/PhysRevB.79.193201

[41] Zagorac D, Schön JC, Zagorac J, Jansen M (2014) Prediction of structure candidates for zinc oxide as a function of pressure and investigation of their electronic properties. Phys Rev B 89:075201. https://doi.org/10.1103/PhysRevB.89.075201

[42] Singh S, Tripathi MN (2016) Enhanced optoelectronic property of ZnO under negative pressure condition: a first-principles study. Mater Res Express 3:086301. https://doi.org/10.1088/2053-1591/3/8/086301

[43] Shabbir S, Shaari A, Ul Haq B, Ahmed R, Ahmed M (2020) Investigations of novel polymorphs of ZnO for optoelectronic applications. Optik 206:164285. https://doi.org/10.1016/j.ijleo.2020.164285

[44] Eom TH, Han JI (2018) Single fiber UV detector based on hydrothermally synthesized ZnO nanorods for wearable computing devices. Appl Surf Sci 428:233–241. https://doi.org/10.1016/j.apsusc.2017.09.127

[45] Liu G, Li Q, Qiu N, He J, Huang Q, Luo K, Lin F, Lin CT, Du S (2016) Structural, electronic and mechanical properties of $(Nb_xTi_{1-x})_2SC$ and $(Nb_xZr_{1-x})_2SC$ ($0\leqslant x\leqslant 1$) from first-principles investigations. Comput Theor Chem 1090:58–66. https://doi.org/10.1016/j.comptc.2016.05.013

[46] Zhou Y, Peng Z, Chen Y, Luo K, Zhang J, Du S (2019) First-principles study of the electronic, optical and transport of few-layer semiconducting MXene. Comput Mater Sci 168:137–143. https://doi.org/10.1016/j.commatsci.2019.05.051

[47] Wu H, Shi XL, Liu WD, Li M, Gao H, Zhou W, Shao Z, Wang Y, Liu Q, Chen ZG (2021) Double perovskite Pr_2-$CoFeO_6$ thermoelectric oxide: roles of Sr-doping and Micro/nanostructuring. Chem Eng J 425:130668. https://doi.org/10.1016/j.cej.2021.130668

[48] Shi XL, Wu H, Liu Q, Zhou W, Lu S, Shao Z, Dargusch M, Chen ZG (2020) $SrTiO_3$-based thermoelectrics: progress and challenges. Nano Energy 78:105195. https://doi.org/10.1016/j.nanoen.2020.105195

[49] Heciri D, Belkhir H, Hamidani A, Bououdina M, Ahuja R (2018) Theoretical investigation of structural, electronic and optical properties of $(BeS)_1/(BeSe)_1$, $(BeSe)_1/(BeTe)_1$ and $(BeS)_1/(BeTe)_1$ superlattices under pressure. Chem Phys Lett 713:71–84. https://doi.org/10.1016/j.cplett.2018.10.008

[50] Majumder R, Hossain MM (2019) First-principles study of structural, electronic, elastic, thermodynamic and optical properties of topological superconductor LuPtBi. Comput Condens Matter 21:e00402. https://doi.org/10.1016/j.cocom.2019.e00402

[51] Benaadad M, Nafidi A, Melkoud S, Khan MS, Soubane D (2021) First-principles investigations of structural, optoelectronic and thermoelectric properties of Cu-based chalcogenides compounds. J Mater Sci 56:15882–15897. https://doi.org/10.1007/s10853-021-06325-y

[52] Mayengbam R, Tripathy SK, Palai G, Dhar SS (2018) First-principles study of phase transition, electronic, elastic and optical properties of defect chalcopyrite $ZnGa_2Te_4$ semiconductor under different pressures. J Phys Chem Solids 119:193–201. https://doi.org/10.1016/j.jpcs.2018.03.027

[53] Sun L, Liu Y, Wu P, Zhou W (2020) Band structure and optical properties of MoS_2/SnO_2 hetero-bilayer from hybrid functional calculations. Mater Chem Phys 239:122071. https://doi.org/10.1016/j.matchemphys.2019.122071

[54] Garwood T, Modine NA, Krishna S (2017) Electronic structure modeling of InAs/GaSb superlattices with hybrid density functional theory. Infrared Phys Tech 81:27–31. https://doi.org/10.1016/j.infrared.2016.12.007

[55] Lee H, Cheong SW, Kim BG (2015) Hybrid functional band gap calculation of SnO_6 containing perovskites and their derived structures. J Solid State Chem 228:214–220. https://doi.org/10.1016/j.jssc.2015.04.022

[56] Tomić S, Montanari B, Harrison NM (2008) The group III–V's semiconductor energy gaps predicted using the B3LYP hybrid functional. Physica E 40:2125–2127. https://doi.org/10.1016/j.physe.2007.10.022

[57] Chronis AG, Sigalas MM, Koukaras EN (2019) Absorption spectrum of magnesium and aluminum hydride nanoparticles. Mater Chem Phys 228:244–253. https://doi.org/10.1016/j.matchemphys.2019.02.081

[58] Huang Y, Yang L, Liu C, Liu X, Liu J, Huang X, Zhu P, Cui T, Sun C, Bao Y (2019) Lasing-mode switch of a hexagonal ZnO pyramid driven by pressure within a diamond anvil cell. J Phys Chem Lett 10:610–616. https://doi.org/10.1021/acs.jpclett.8b03748

[59] Chayka IF, Sobolev AV, Izokh AE, Batanova VG, Krasheninnikov SP, Chervyakovskaya MV, Kontonikas-Charos A, Kutyrev AV, Lobastov BM, Chervyakovskiy VS (2020) Fingerprints of kamafugite-like magmas in mesozoic lamproites of the aldan shield: evidence from olivine and olivine-hosted inclusions. Miner 10:337. https://doi.org/10.3390/min10040337

[60] Mao P, Yu B, Liu Z, Wang F, Ju Y (2013) First-principles calculation of electronic structure and elastic property of AB_2 type intermetallics in Mg-Zn-Ca alloy. Acta Metall Sinica 49:1227–1233. https://doi.org/10.3724/SP.J.1037.2013.00266

[61] Ceperley DM, Alder BJ (1980) Ground state of the electron gas by a stochastic method. Phys Rev Lett 45:566–569. https://doi.org/10.1103/PhysRevLett.45.566

[62] Parrinello M, Rahman A (1980) Crystal structure and pair potentials: a molecular-dynamics study. Phys Rev Lett 45:1196–1199. https://doi.org/10.1103/PhysRevLett.45.1196

[63] Kresse G, Joubert D (1999) From ultrasoft pseudopotentials to the projector augmented-wave method. Phys Rev B 59:1758–1775. https://doi.org/10.1103/PhysRevB.59.1758

[64] Pfrommer BG, Cote M, Louie SG, Cohen ML (1997) Relaxation of crystals with the quasi-Newton method. J Comput Phys 131(1997):233–240. https://doi.org/10.1006/jcph.1996.5612

[65] Bauernschmitt R, Ahlrichs R (1996) Treatment of electronic excitations within the adiabatic approximation of time dependent density functional theory. Chem Phys Lett 256:454–464. https://doi.org/10.1016/0009-2614(96)00440-X

[66] Mang A, Reimann K, Rübenacke S (1995) Band gaps, crystal-field splitting, spin-orbit coupling, and exciton binding energies in ZnO under hydrostatic pressure. Solid State Commun 94:251–254. https://doi.org/10.1016/0038-1098(95)00054-2

[67] Vinet P, Ferrante J, Smith JR, Rose JH (1986) A universal equation of state for solids. J Phys C 19:L467–L473. https://doi.org/10.1088/0022-3719/19/20/001

[68] Liang CP, Gong HR (2013) Atomic structure, mechanical quality, and thermodynamic property of TiH_x phases. J Appl Phys 114:043510. https://doi.org/10.1063/1.4816485

[69] Jacobs K, Schulz D, Klimm D, Ganschow S (2010) Melt growth of ZnO bulk crystals in Ir crucibles. Solid State Sci 1:307–310. https://doi.org/10.1016/j.solidstatesciences.2009.05.015

[70] Seko A, Oba F, Kuwabara A, Tanaka I (2005) Pressure-induced phase transition in ZnO and ZnO-MgO pseudobinary system: a first-principles lattice dynamics study. Phys Rev B 72:024107. https://doi.org/10.1103/PhysRevB.72.024107

[71] Wu HY, Cheng XL, Hu CH, Zhou P (2010) The structure and thermodynamic properties of zinc oxide with wurtzite and rocksalt structure under high pressures. Physica B 405:606–612. https://doi.org/10.1016/j.physb.2009.09.074

[72] Huang MH, Mao S, Feick H, Yan HQ, Wu YY, Kind H, Weber E, Russo R, Yang PD (2001) Room-temperature ultraviolet nanowire nanolasers. Science 292:1897–1899. https://doi.org/10.1126/science.1060367

[73] Dong CL, Persson C, Vayssieres L, Augustsson A, Schmitt T, Mattesini M, Ahuja R, Chang CL, Guo JH (2004) Electronic structure of nanostructured ZnO from x-ray absorption and emission spectroscopy and the local density approximation. Phys Rev B 70:195325. https://doi.org/10.1103/PhysRevB.70.195325

[74] Clark SJ, Robertson J, Lany S, Zunger A (2010) Intrinsic defects in ZnO calculated by screened exchange and hybrid density functionals. Phys Rev B 81:115311. https://doi.org/10.1103/PhysRevB.81.115311

[75] Gerosa M, Bottani CE, Di Valentin C, Onida G, Pacchioni G (2018) Accuracy of dielectric-dependent hybrid functionals in the prediction of optoelectronic properties of metal oxide semiconductors: a comprehensive comparison with many-body GW and experiments. J Phys 30:044003. https://doi.org/10.1088/1361-648X/aa9725

[76] Gerosa M, Bottani CE, Caramella L, Onida G, Di Valentin C, Pacchioni G (2015) Electronic structure and phase stability of oxide semiconductors: Performance of dielectric-dependent hybrid functional DFT, benchmarked against GW band structure calculations and experiments. Phys Rev B 91:155201. https://doi.org/10.1103/PhysRevB.91.155201

[77] Schleife A, Fuchs F, Furthmuller J, Bechstedt F (2006) First-principles study of ground- and excited-state properties of MgO, ZnO, and CdO polymorphs. Phys Rev B 73:245212. https://doi.org/10.1103/PhysRevB.73.245212

[78] Zhang XD, Guo ML, Li WX, Liu CL (2008) First-principles study of electronic and optical properties in wurtzite $Zn_{1-x}Cd_xO$. J Appl Phys 103:091914. https://doi.org/10.1063/1.2901033

Publisher's Note Springer Nature remains neutral with regard to jurisdictional claims in published maps and institutional affiliations.

Springer Nature or its licensor holds exclusive rights to this article under a publishing agreement with the author(s) or other rightsholder(s); author self-archiving of the accepted manuscript version of this article is solely governed by the terms of such publishing agreement and applicable law.